Article

Cell Reports

Post-translational Modifications of OLIG2 Regulate Glioma Invasion through the TGF-β Pathway

Graphical Abstract

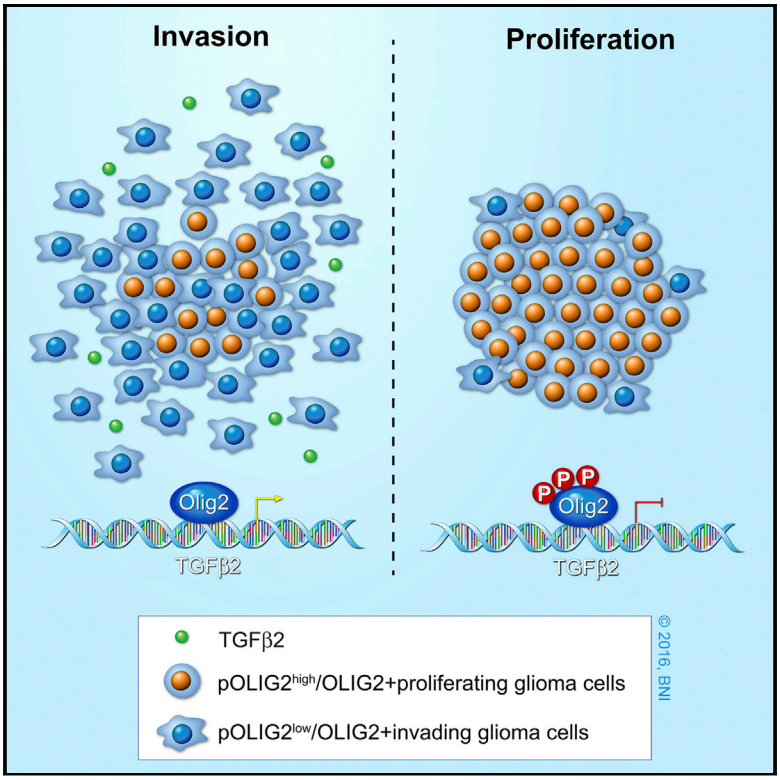

Highlights

- Glioma cells expressing unphosphorylated OLIG2 are highly invasive
- Unphosphorylated OLIG2 upregulates the TGF-β2 pathway and activates invasion genes
- Inhibition of the TGF-β pathway blocks OLIG2-mediated invasion
- Phospho-OLIG2 suppresses TGF-β2-mediated invasion

Authors

Shiv K. Singh, Roberto Fiorelli, Robert Kupp, ..., Michael E. Berens, Nader Sanai, Shwetal Mehta

Correspondence

shwetal.mehta@dignityhealth.org

In Brief

Singh et al. show that the phosphorylation status of a CNS-specific transcription factor, OLIG2, dictates the switch from the proliferative to invasive phenotype in glioblastoma. Unphosphorylated OLIG2 induces invasion through upregulation of the TGF-β2 pathway. The authors provide a putative mechanism through which OLIG2 regulates both proliferation and invasion in GBM cells.

Singh et al., 2016, Cell Reports *16*, 950–966
July 26, 2016
http://dx.doi.org/10.1016/j.celrep.2016.06.045

OPEN ACCESS
CellPress

Cell Reports
Article

Post-translational Modifications of OLIG2 Regulate Glioma Invasion through the TGF-β Pathway

Shiv K. Singh,[1] Roberto Fiorelli,[1] Robert Kupp,[1] Sindhu Rajan,[1] Emily Szeto,[1] Costanza Lo Cascio,[1] Cecile L. Maire,[2] Yu Sun,[3] John A. Alberta,[3] Jennifer M. Eschbacher,[4] Keith L. Ligon,[2] Michael E. Berens,[5] Nader Sanai,[1] and Shwetal Mehta[1,*]

[1]Division of Neurobiology, Barrow Brain Tumor Research Center, Barrow Neurological Institute, St. Joseph's Hospital and Medical Center, Phoenix, AZ 85013, USA
[2]Department of Pathology, Brigham and Women's Hospital, Harvard Medical School, Boston, MA 02115, USA
[3]Department of Cancer Biology, Dana-Farber Cancer Institute, Boston, MA 02115, USA
[4]Division of Neuropathology, Barrow Neurological Institute, St. Joseph's Hospital and Medical Center, Phoenix, AZ 85013, USA
[5]Cancer and Cell Biology Division, Translational Genomics Institute, Phoenix, AZ 85004, USA
*Correspondence: shwetal.mehta@dignityhealth.org
http://dx.doi.org/10.1016/j.celrep.2016.06.045

SUMMARY

In glioblastoma, invasion and proliferation are presumed to be mutually exclusive events; however, the molecular mechanisms that mediate this switch at the cellular level remain elusive. Previously, we have shown that phospho-OLIG2, a central-nervous-system-specific transcription factor, is essential for tumor growth and proliferation. Here, we show that the modulation of OLIG2 phosphorylation can trigger a switch between proliferation and invasion. Glioma cells with unphosphorylated OLIG2$^{S10,\ S13,\ S14}$ are highly migratory and invasive, both in vitro and in vivo. Mechanistically, unphosphorylated OLIG2 induces TGF-β2 expression and promotes invasive mesenchymal properties in glioma cells. Inhibition of the TGF-β2 pathway blocks this OLIG2-dependent invasion. Furthermore, ectopic expression of phosphomimetic Olig2 is sufficient to block TGF-β2-mediated invasion and reduce expression of invasion genes (ZEB1 and CD44). Our results not only provide a mechanistic insight into how cells switch from proliferation to invasion but also offer therapeutic opportunities for inhibiting dissemination of gliomas.

INTRODUCTION

Glioblastoma (GBM) is the most aggressive, infiltrative, and lethal brain tumor in adults, with a median survival of 9–14 months after diagnosis (Furnari et al., 2007; Maher et al., 2001; Ostrom et al., 2015). Although relatively rare, these tumors are associated with high mortality rates, mainly due to their invasive nature and resistance to radiotherapy and chemotherapy. The tumors almost always recur, and no standard-of-care treatment is available for recurrent GBM (Hess et al., 1999; Wong et al., 1999; Weller et al., 2013). One reason for tumor recurrence is the presence of highly tumorigenic and invasive cells that infiltrate normal brain parenchyma and evade surgical resection (Giese et al., 2003). Hence, the development of effective therapies for GBM requires an understanding of the mechanisms that trigger invasive phenotypes in GBM tumors.

The GBM peritumoral zone is composed of invasive cells with distinct molecular phenotypes that are highly migratory and that infiltrate the healthy brain (Giese et al., 1996; Glas et al., 2010; Silver et al., 2013). Several studies have shown that cell proliferation and migration/invasion are mutually exclusive events, with proliferating cells being less motile and with rapidly moving cells proliferating slowly (Giese, 2003; Giese et al., 1996; Cayre et al., 2009). Genes involved in cell migration have been shown to be upregulated in invading cells at the tumor rim, whereas proliferation genes are downregulated (Dhruv et al., 2013; Loftus et al., 2012). This difference in gene expression suggests a possible role for transcription factors (TFs) in modulating cellular phenotype from proliferation to invasion. Several TFs (e.g., ZEB1, STAT3, C/EBPβ, and TAZ) have been shown to play a critical role in the induction of invasive mesenchymal phenotypes in GBM cells (Carro et al., 2010; Siebzehnrubl et al., 2013). Herein, we will demonstrate how a central nervous system (CNS)-specific TF, OLIG2, can promote either invasion or proliferation based on its phosphorylation state.

Olig2 is a basic helix-loop-helix (bHLH) TF expressed in the multipotent neural progenitor cells in the developing brain and is required for the generation of oligodendrocytes and certain subtypes of motor neurons (Meijer et al., 2012). During CNS development, Olig2 performs two contrasting functions: early on, Olig2 sustains the replication competence of progenitor cells, and later, when a sufficient number of progenitor cells are reached, Olig2 is required for cell-type specification of oligodendrocytes and motor neurons (Meijer et al., 2012). In the adult brain, Olig2 is not only expressed in mature oligodendrocytes but is also expressed in the two proliferating populations of cells, namely, the transit-amplifying type C cells and the NG2-positive

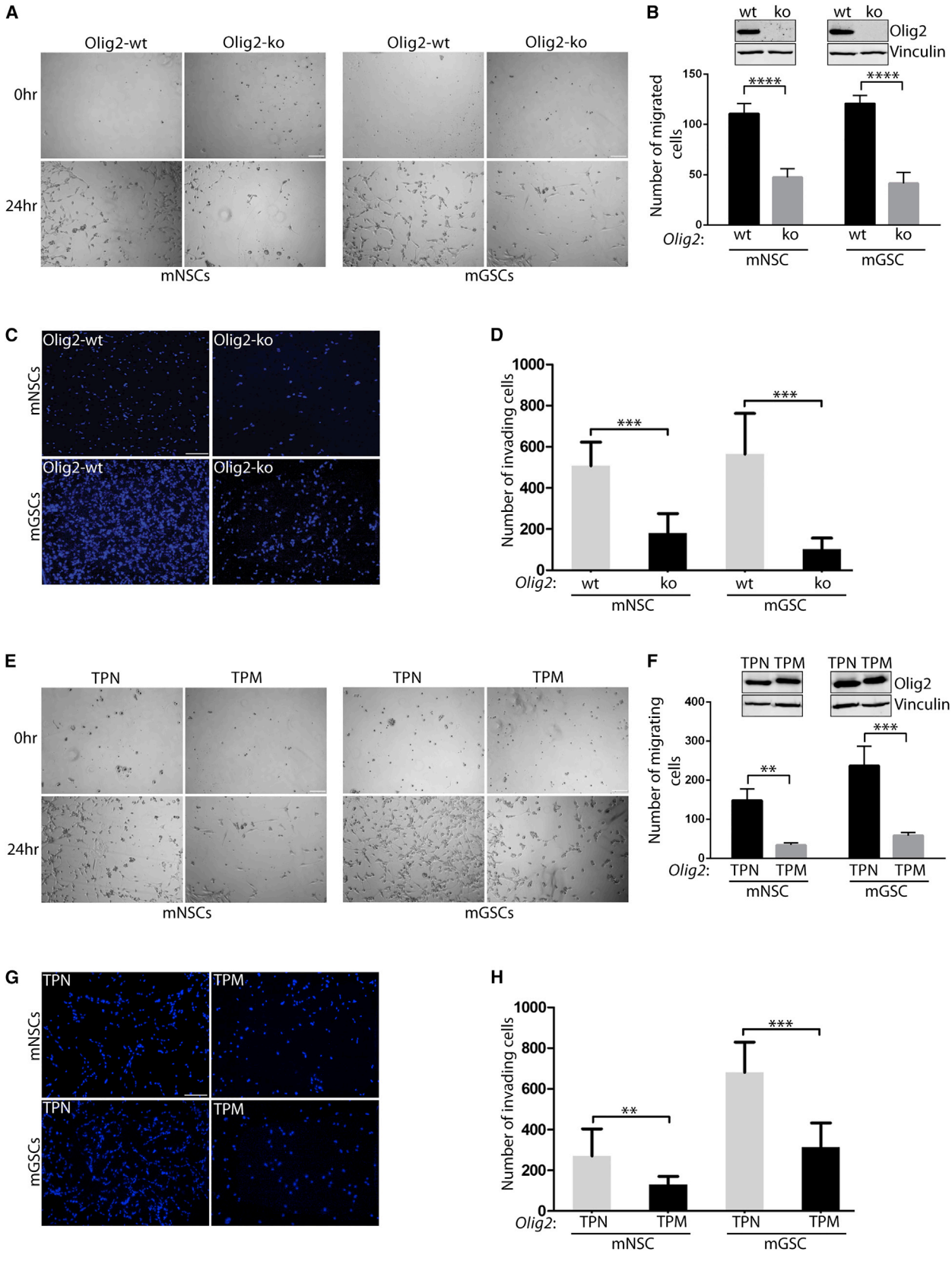

(legend on next page)

glia (Meijer et al., 2012). A pathological correlate of this proliferative function of Olig2 is observed in high-grade gliomas. OLIG2 has been shown to be universally expressed in almost all diffuse gliomas (Ligon et al., 2004; Lu et al., 2001). Apart from marking glioma cells, Olig2 expression is required for glioma growth, which has been both demonstrated in a genetically relevant murine model and in orthotopic patient-derived xenograft models (Ligon et al., 2007; Mehta et al., 2011). Recently, OLIG2 was shown to be a key TF required for reprogramming differentiated glioma cells into highly tumorigenic glioma stem-like cells (GSCs) (Suvà et al., 2014).

Olig2 is phosphorylated at the triple-serine motif (S10, S13, and S14) near the amino terminus (pOlig2) (Sun et al., 2011). The phosphorylation at these sites is developmentally regulated and present in cycling neural progenitor cells, but not in mature oligodendrocytes (Sun et al., 2011). Most GSCs express pOLIG2 at levels similar to those of cycling progenitor cells. Expression of a triple-phosphomimetic (TPM) mutant of Olig2 leads to faster tumor growth than does expression of a triple-phosphonull (TPN) mutant in a genetically relevant murine glioma model. TPN-expressing cells are able to form tumors, but with longer latency (Sun et al., 2011).

Recent studies have shown that Olig2 might play a role in promoting migration/invasion in normal oligodendrocyte precursor cells (OPCs), as well as in GSCs (Hornig et al., 2013; Nevo et al., 2014). In addition, recent findings suggest that both contrast-enhancing GBM tumor core, as well as non-enhancing tumor margins, express high levels of Olig2 (Venere et al., 2015). An important question that then arises is how a single TF, such as OLIG2, regulates these distinct transcriptional programs of proliferation and invasion. In this study, we demonstrate how the N-terminal phosphorylation of OLIG2 can regulate cell invasion through its transcriptional regulation of the TGF-β2 pathway. We show that cells expressing unphosphorylated $Olig2^{S10,\ 13,\ 14}$ or low levels of pOLIG2 ($pOLIG2^{low}$) are highly invasive. Furthermore, we find that inhibition of the TGF-β2 pathway suppresses OLIG2-mediated invasion.

RESULTS

Olig2 Is Required for Migration/Invasion of Both Normal Neural Stem Cells and Glioma Stem-like Cells

To interrogate the role of Olig2 in promoting cell migration/invasion, we compared murine Olig2-KO (Olig2-knockout) and Olig2-WT (Olig2-wild-type) using an in vitro migration assay. We utilized previously characterized murine glioma stem-like cells (mGSCs) (*Ink4a/Arf*$^{-/-}$ *hEGFRvIII*) and normal murine neural stem cells (mNSCs) (Ligon et al., 2007). Both mNSCs and mGSCs expressing wild-type Olig2 showed increased capacity of migration compared to cells without Olig2 (Olig2-KO) (Figures 1A and 1B). There was no significant difference in cell viability or substrate attachment between Olig2-WT and Olig2-KO mNSCs and mGSCs in samples collected 2 hr post-plating (Figure S1A). However, after 24 hr, Olig2-WT cells proliferate at slightly higher (but significant) efficiency compared to Olig2-KO cells (Figure S1B). Next, through a 3D Matrigel matrix, we assessed whether Olig2 expression is also required for cell invasion. As shown in Figures 1C and 1D, under both normal and oncogenic backgrounds, Olig2-WT cells have a significantly higher capability to invade through a 3D matrix than do Olig2-KO cells. It is known that the absence of Olig2 produces a small but significant effect on the proliferation rate of normal and oncogenic neurospheres (Ligon et al., 2007). Thus, the question is whether the increase in cell invasion is due to the increased proliferation of Olig2-WT cells. However, considering that Olig2-WT and Olig2-KO have doubling times of 33 and 43 hr (Ligon et al., 2007), respectively, the increased invasion observed after 24 hr is highly unlikely to be solely due to higher proliferation rates.

N-Terminal Phosphorylation of Olig2 at a Triple-Serine Motif Affects Migration/Invasion of mNSCs and mGSCs

We used previously established Olig2-TPM and TPN mutant-expressing cell lines to examine the effect of Olig2 phosphorylation on the ability of mNSCs and mGSCs to migrate/invade (Sun et al., 2011). We found that highly proliferative TPM-expressing murine cells migrate and invade significantly more slowly than TPN-expressing cells (Figures 1E–1H). Control experiments confirmed that the differences in migration and invasion between TPM and TPN mutants are independent of cell viability or loss of attachment (Figures S1C and S1D). As previously observed (Sun et al., 2011), there were significantly more TPM cells after 24 hr of seeding than TPN cells. These data demonstrate that both mNSCs and mGSCs expressing the unphosphorylated form of Olig2 have increased migration/invasion ability in vitro.

Phosphorylation Level of OLIG2 at Triple Serine Motif Dictates Migration/Invasion Ability of Human GSCs

Our previous studies show that OLIG2 is phosphorylated at the N terminus in most proliferating GBM cells grown in the presence of growth factors (Sun et al., 2011). However, the phosphorylation levels significantly vary among various human patient-derived GBM GSCs (hGSCs), as seen previously (Sun et al., 2011), and from the pOLIG2/total OLIG2 (tOLIG2) levels across the six hGSC lines used in this study (Figures 2A and S2A; Table

Figure 1. Phosphorylation Status of Olig2 Affects Invasion/Migration of mNSCs and mGSCs

(A–D) Olig2-WT mNSCs and mGSCs are more migratory and invasive than Olig2-KO cells. Representative images of the central zone to which cells migrate at 0 and 24 hr (A) and quantification of the total number of migrated cells at 24 hr (B). Inset shows the western blot data for Olig2 and Vinculin. Representative images are from transwell assays of mNSCs and mGSCs with or without Olig2 after 24 hr post-seeding (C) and show quantification of the total number of DAPI-stained nuclei (D).

(E–H) In vitro migration/invasion assays of mNSC- and mGSC-expressing Olig2 phosphomutants. mNSC- or mGSC-expressing TPN mutant shows the increased migration (E and F) and invasion (G and H) compared to the TPM-expressing cells. (G) IRS quantification of Ki67+ (red) cells at core, edge and rim regions. (H) IRS quantification of pSMAD2+ (green) cells at core, edge and rim regions. Scale bars, 100 μm. Inset in (F) shows western blot probed for Olig2 and Vinculin. For all bar graphs, the data represent mean ± SD of three independent experiments. *$p < 0.05$; **$p < 0.01$; ***$p < 0.001$.

See also Figure S1.

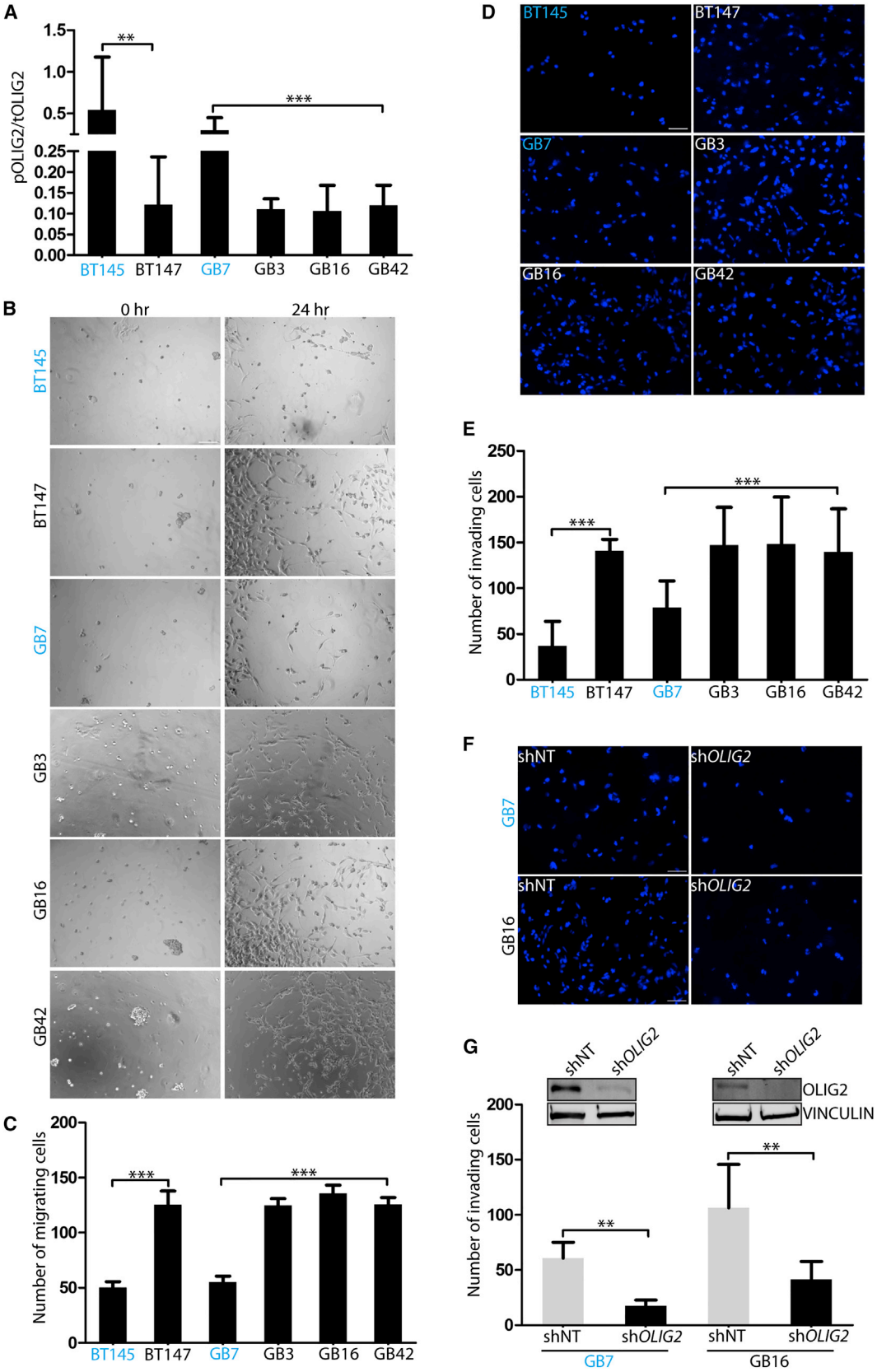

(legend on next page)

S1). As shown in Figures 2B and 2C, the phosphorylation levels of OLIG2 affect the migration/invasion capacity of multiple hGSCs. There is a significant difference in the number of migrating hGSCs with pOLIG2^{high} (BT145 and GB7, labeled in blue) than hGSCs with pOLIG2^{low} (BT147, GB3, GB16, and GB42). We observed similar differences between hGSCs in their ability to invade the 3D matrix (Figures 2D and 2E). As expected, hGSCs with pOLIG2^{high} were more proliferative than those with pOLIG2^{low}, and no difference was observed in substrate attachment and cell viability (Figures S2B and S2C).

To determine whether increased invasion in hGSCs is dependent on OLIG2 expression, we transduced three hGSCs (GB7, GB16, and BT147) with either a control non-target short hairpin RNA (shNT) or sh*OLIG2*. Knockdown of *OLIG2* significantly decreased the ability of all three hGSCs to invade (Figures 2F, 2G, and S2D). Knockdown with a second hairpin targeting different regions of OLIG2 ORF confirmed that the decrease in invasion was not an off-target effect (Figure S2E). Thus, it can be concluded that OLIG2 expression promotes cell migration/invasion in hGSCs and that the phosphorylation status of OLIG2 is critical in determining their invasive properties in vitro.

Glioma Cells Expressing Unphosphorylated OLIG2 Are Invasive

We compared the peritumoral rims in tumors induced by TPN- and TPM-expressing mGSCs to assess whether unphosphorylated Olig2 expression promotes invasion in vivo. As indicated in Figures 3A, 3B, and S3A–S3D, TPN cells could be detected in the normal brain regions distal from the tumor core, whereas TPM cells showed restricted invasion of the brain parenchyma. Quantification of the number of cells that invaded the adjacent areas, e.g., the tumor rim, ventricles, the white matter tracts, and the dentate gyrus (DG) region, clearly demonstrated the invasive nature of TPN cells (Figure 3C). In addition, TPN cells showed strong expression of Snail/Slug (EMT marker) compared to TPM-induced tumors (Figure S3E).

In order to further strengthen our observations with genetically defined murine glioma models and Olig2 phosphomutants, we compared patient-derived xenograft (PDX) tissues from the hGSC lines BT147 (pOLIG2^{low}) and BT145 (pOLIG2^{high}) and probed them with the stem cell marker VIMENTIN (VIM) to track hGSCs. Immunostaining of the BT147 xenograft revealed extensive infiltration of tumor cells throughout the brain parenchyma, while BT145 cells were comparatively more localized (Figures 3D and 3E). To confirm that the VIM+ cells were indeed tumor cells, we co-stained them with a human-specific NESTIN antibody that colocalized with VIM in both BT147 and BT145 tumors, except in the ventricular regions of BT145 tumor (Figures 3F and 3G). VIM+ and NESTIN+ BT147 cells were detected within the DG area as well (Figure S3F). Furthermore, we saw strong ZEB1 expression in the invasive BT147 xenograft, including the ventricular and DG areas (Figures 3H, 3I, and S3G), but only a few ZEB1+ cells were seen in the BT145 tumor tissue.

To further examine differences in tumor cell dispersion between pOLIG2^{high} and pOLIG2^{low} hGSCs, we examined brain tissues from GB3, BT145, and GB16 PDXs at an early time point (3 weeks) post-implantation. The pOLIG2^{low} lines GB3 and GB16 cells migrated significantly further from the graft site, mostly along the white matter tracts, compared to pOLIG2^{high} BT145 cells, which were restricted to the site of injection (Figures 4A–4E and S4A). These data strongly support our claim that pOLIG2^{low} hGSCs are highly invasive, both in vitro and in vivo.

To analyze the localization of phosphorylated and total OLIG2 within human GBM specimens, we stained fresh frozen tissue sections from multiple GBM patients for pOLIG2, tOLIG2, and Ki67. As previously reported, we found that almost all Ki67+ cells are OLIG2+; however, a larger percentage (~70%) of OLIG2+ cells do not express Ki67 (Figures 4F and 4G) (Ligon et al., 2004, 2007). Using our highly specific pOLIG2 antibody, we found that pOLIG2 co-localizes with the proliferative marker Ki67 in ~90% of cells (Figures 4H and 4I), confirming our previous observations (Ligon et al., 2007; Sun et al., 2011). Within multiple GBM tissues, we found a decreasing gradient of pOLIG2+ cells from the tumor core to the invasive edge (Figures 4I and S4B–S4D). These data support our hypothesis that proliferating cells express pOLIG2, and invading cells express unphosphorylated OLIG2.

To assess the distribution of OLIG2+ and pOLIG2+ cells within GBM tumors, we probed a GBM tissue microarray (TMA) comprising 33 matched GBM tumor core, edge, and rim tissues (Kislin et al., 2009). Since our pOLIG2 antibody does not work on paraffin-embedded tissues (and there is ~90% colocalization between pOLIG2 and Ki67), we utilized Ki67 staining as a surrogate for pOLIG2 staining on paraffin-embedded tissues. In a vast majority of GBM tissues, OLIG2+ cells were detected at the tumor core, edge, and infiltrative tumor rim, whereas Ki67+ (pOLIG2) cells were predominantly found at the tumor core (Figures 4J and 4K). These data strongly suggest that Ki67+ (pOLIG2+) proliferating cells are mainly present at the tumor core, whereas unphosphorylated OLIG2-expressing cells are present throughout the tumor.

OLIG2 Phosphorylation Regulates Expression of Invasion Genes

Since OLIG2 is a TF, we investigated the effect of OLIG2 phosphorylation on genes involved in invasion, cell-cycle regulation,

Figure 2. N-Terminal Phosphorylation of OLIG2 Affects Invasion/Migration in hGSCs

(A) Indicated hGSC lysates were analyzed for the ratio of pOLIG2 over tOLIG2 by immunoblotting with pOLIG2, OLIG2, and VINCULIN antibodies. pOLIG2^{high} hGSCs are labeled in blue.

(B–E) In vitro cell migration assays show that cell lines with pOLIG2^{low} (BT147, GB3, GB16, and GB42) are more migratory (B and C) and invasive (D and E) compared to cell lines with pOLIG2^{high} (BT145 and GB7).

(F and G) Knockdown of *OLIG2* reduces glioma cell invasion. Invasion assay was performed 72 hr post-transduction of GB7 and GB16 cells with either control non-target hairpin (shNT) or sh*Olig2*-expressing lentivirus (F). Quantification of the total number of invading cells after knockdown of *OLIG2* (G) is shown. Western blot analysis after *OLIG2* knockdown in GB7 and GB16 cells (G, inset). Scale bars, 100 (B) and 50 μm (D and F). For all bar graphs, the data represent mean ± SD of three independent experiments.*$p < 0.05$; **$p < 0.01$; ***$p < 0.001$.

See also Figure S2.

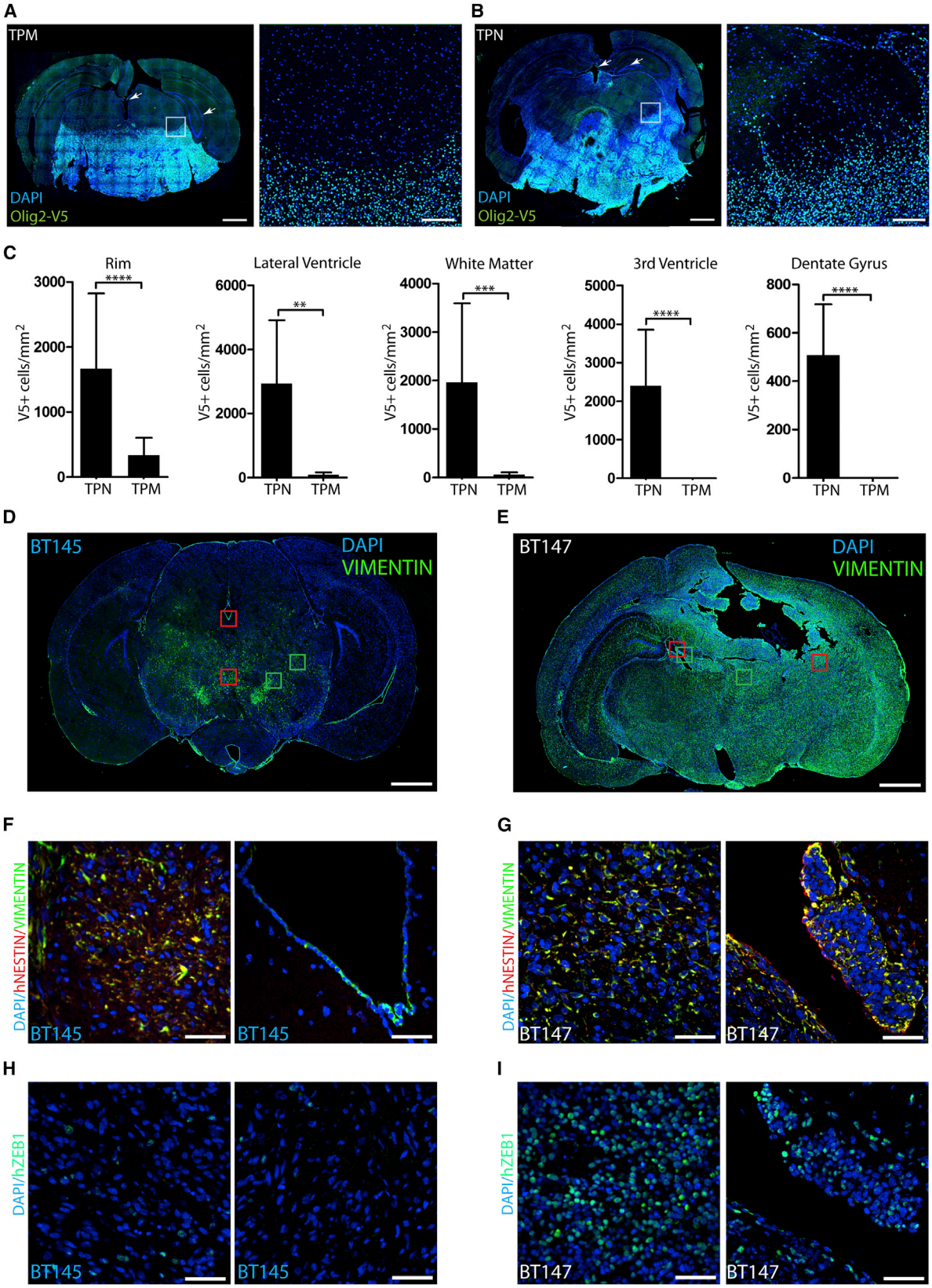

(legend on next page)

and proliferation. We performed qRT-PCR analysis of invasion-related markers enriched for genes associated with an epithelial-to-mesenchymal transition (EMT) (e.g., *TWIST1*, *CD44*, *TGFβ2*, *CREB1*, and *ZEB1*) (Kalluri and Weinberg, 2009; Polyak and Weinberg, 2009) in mGSCs and hGSCs. Interestingly, we found that invasion genes are upregulated in TPN-expressing mGSCs compared to TPM-expressing cells. Expression of *Tgfβ2*, *Zeb1*, and *Cd44* was upregulated in TPN-expressing mGSCs, and proliferation markers (*Egfr* and *Cdk6*) were highly expressed in TPM-expressing cells (Figures S5A and S5B). Next, we examined whether this observation also holds true in hGSCs and whether it is dependent on OLIG2 phosphorylation status. qRT-PCR analysis showed a robust transcriptional upregulation of invasion genes in hGSCs with pOLIG2^{low} (BT147 and GB16) compared to hGSCs with pOLIG2^{high} (BT145 and GB7) (Figures 5A and 5B). In contrast, proliferation and cell-cycle-associated genes were upregulated in pOLIG2^{high} hGSCs (Figures S5C and S5D). To further confirm that OLIG2 regulates the expression of invasion genes, we ablated OLIG2 expression in BT147, GB16, and GB7 cells. shRNA-mediated knockdown of *OLIG2* led to a significant decrease in the expression of invasion genes in all three hGSCs, suggesting that OLIG2 is required for the regulation of expression of these genes in hGSCs (Figures 5C, 5D, and S5E). Previous studies have shown that ZEB1 regulates OLIG2 expression. Our data demonstrate a reciprocal regulation of ZEB1 by OLIG2. Analysis of published chromatin immunoprecipitation sequencing (ChIP-seq) data (Suvà et al., 2014) showed that OLIG2 associated with an enhancer region of the ZEB1 gene, which is also enriched for H3K27ac mark. Directed ChIP analysis in the GB16 line (pOLIG2^{low}) confirmed that OLIG2 associated with the ZEB1 enhancer region and that the region is also marked by H3K27ac (Figure S5F). Furthermore, ZEB1 expression is dramatically reduced after knockdown of *OLIG2* in two hGSCs (GB3 and GB16) (Figure S5G). Collectively, these data show that unphosphorylated Olig2, or pOLIG2^{low}, induces the expression of migration/invasion genes.

OLIG2 Promotes Invasion by Upregulating *TGFβ2* Expression

To scrutinize the downstream mechanisms through which OLIG2 governs invasion, we focused our attention on TGF-β2 for two reasons: *Tgfβ2* is a direct genetic target of Olig2 in normal neural progenitor cells (Meijer et al., 2014), and the TGF-β pathway plays an important role in the invasion of tumor cells in several solid cancers, including GBM (Anido et al., 2010; Rich, 2003; Weller et al., 2001; Wick et al., 2001). Analysis of ChIP-seq tracks from Meijer et al. (2014) demonstrated that both phosphorylated and unphosphorylated forms of Olig2 associate with the *Tgfβ2* locus (Figures 5E and 5F) and regulate its expression in normal neural progenitor cells. A ChIP assay with Olig2 and H3K27ac antibodies confirmed association of both TPM and TPN mutants with *Tgfβ2* enhancer region in mGSCs (Figure 5F), and we found significant enrichment of the active enhancer histone mark (H3K27ac) at the *Tgfβ2* locus (ChIP-seq track for H3K27ac from Mateo et al. 2015) in TPN cells compared to that in TPM cells (Figures 5E and 5F).

By performing a ChIP assay in hGSCs, we confirmed that TGF-β2 is also a direct target of OLIG2 in hGSCs. OLIG2 associated with *TGFβ2* locus in hGSCs within a region that has been shown to be enriched for H3K27ac marks (Suvà et al., 2014) (Figures 5G and 5H). We performed ELISA and a TGF-β growth inhibition assay and found that pOLIG2^{low} hGSCs and TPN-expressing murine cells express high levels of TGF-β2 (Figures S6A and S6B). Using TGF-β-sensitive CCL64 cells, we observed significant growth inhibition after incubation with supernatants from pOLIG2^{low} hGSCs or TPN-expressing cells (Figures S6C and S6D) compared to media alone or supernatant from pOLIG2^{high} and TPM-expressing cells. Pre-incubation of the supernatant with the TGF-β2 antibody decreased growth inhibition. These data suggest that *Tgfβ2* expression is upregulated in the presence of unphosphorylated Olig2.

We confirmed that the increase in TGF-β2 levels translates to an increase in downstream TGF-β2 signaling. A TGF-β2 ligand associates with TGF-β type I/II receptors and triggers phosphorylation of SMAD2/3 proteins. Phosphorylated SMAD2/3 (pSMAD2/3) then associates with SMAD4 to form a co-regulatory complex to activate downstream genetic targets (Schmierer and Hill, 2007). We did not detect any difference in TGF-β type I/II receptor expression between pOLIG2^{high} and pOLIG2^{low} lines (Figure S6E). However, we did detect high levels of pSMAD2 expression in oncogenic TPN-induced tumor tissues compared to TPM-induced tumors (Figures 6A and 6B). The correlation between pSMAD2 levels and OLIG2 phosphorylation status in human tumors was confirmed by staining GB7 and GB16 patient tissues with pSMAD2 and Ki67 antibodies. GB16 tissue showed high levels of pSMAD2 compared to GB7 tissue (Figure S6F). We confirmed this pattern by immunostaining of concomitant sections from another fresh frozen human GBM tissue with pSMAD2/Ki67 and pSMAD2/OLIG2 antibodies (Figure 6C). We found very little overlap in pSMAD2 and Ki67 staining; however, most OLIG2+ cells were pSMAD2+. Furthermore, we found that hGSCs with pOLIG2^{low} (GB16 and GB42) had higher levels of

Figure 3. Cells Expressing Unphosphorylated Olig2/ pOLIG2^{low} Are Invasive

(A–C) mGSCs expressing the TPN mutant form highly infiltrative tumors compared to TPM-expressing mGSCs. Immunostaining for V5 epitope tag (green) in murine TPM-expressing tumors (DAPI, blue) is shown (A). TPN-expressing tumors show infiltration of normal brain parenchyma and the ventricular and hippocampal area (arrows) (B). (C) Scale bars, 1 mm and 100 μm. Quantification of invading tumor cells at the peritumoral rim (the area comprised in white boxes in A and B, ventricular areas, white matter tracts, and dentate gyrus regions (C) (arrows) is shown.

(D–I) Tumors induced by hGSCs with pOLIG2^{high} (BT145) are less invasive compared to pOLIG2^{low} (BT147). Immunostaining with anti-VIMENTIN (green) in human GBM xenograft tissues derived from BT145 (D) or BT147 (E) (DAPI, blue). Scale bars, 1 mm. Tracking tumor cells with human-specific NESTIN in PDX tissues (F and G). Images of hNESTIN (red) and VIMENTIN (green) immunostaining in BT145 tumor tissue (zoom-in images of red boxed regions from (D) and (F). Images of hNESTIN immunostaining in BT147 tumor tissue (zoom-in of red boxed regions from (E) and (G) (DAPI, blue). (H and I) Immunostaining with anti-hZEB1 in BT145 (H) and BT147 (I) tissues (zoom-in images of green boxed regions from D and E) is shown. For all bar graphs, data represent mean ± SD of three independent experiments.*$p < 0.05$; **$p < 0.01$; ***$p < 0.001$.

See also Figure S3.

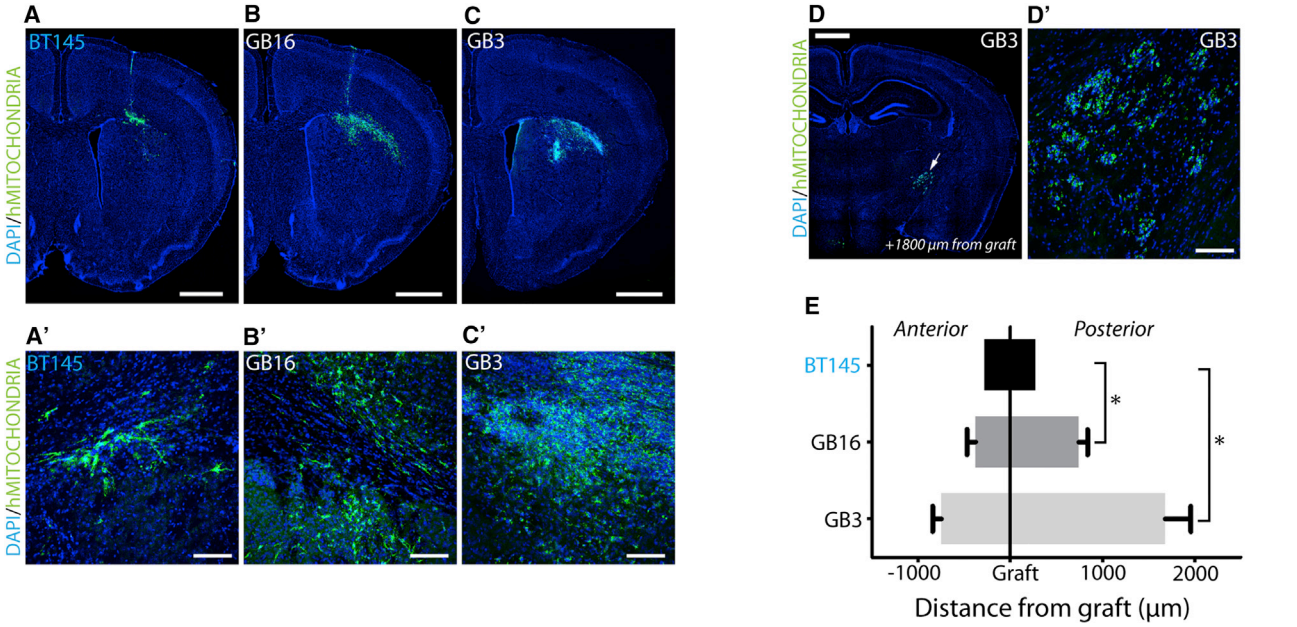

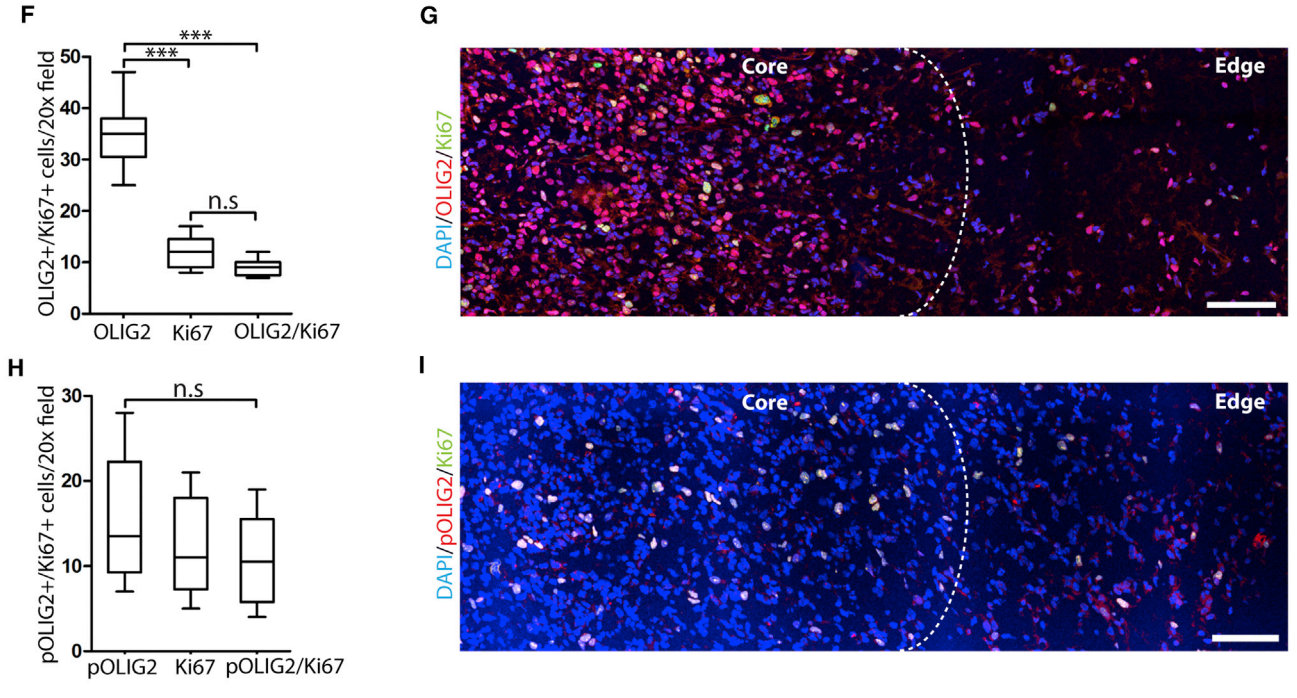

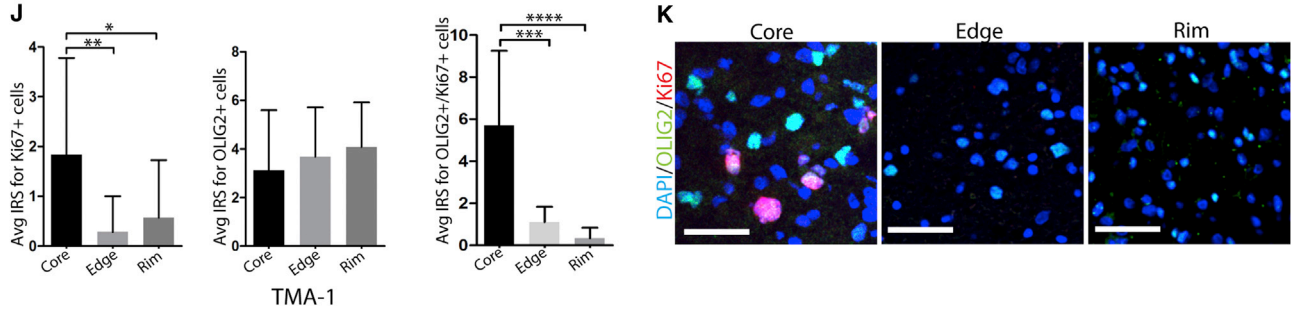

(legend on next page)

pSMAD2 compared to the hGSCs with pOLIG2^{high} (GB7) (Figure 6D). Ablation of OLIG2 (sh*OLIG2*) in GB16 resulted in a decrease in the levels of pSMAD2 (Figure 6E). Next, we probed the TMA with pSMAD2/Ki67 antibodies to assess its localization within the tumor. Similar to OLIG2+ cells (Figure 3), pSMAD2+ cells were found at the tumor core, edge, and rim regions (Figures 6F–6H). We observed no colocalization between pSMAD2 and Ki67. We also immunostained the TMA with OLIG2 and pSMAD2 and found that OLIG2+ and pSMAD2+ cells were present throughout the tumor (Figure S6G).

In breast cancer, TGF-β has been shown to increase the population of cells expressing CD44, a marker known to be upregulated on induction of EMT (Gupta et al., 2009; Mani et al., 2008). Recent studies have demonstrated that in GBM, TGF-β regulates *CD44* expression through induction of ID1 (inhibitor of DNA binding 1 protein) (Anido et al., 2010). We found that an OLIG2-mediated increase in *TGFβ2* expression also correlates with increased CD44 levels. We probed for CD44 levels in the hGSC line with pOLIG2^{high} levels (GB7) and in two hGSC lines with pOLIG2^{low} (GB16 and GB42). Both the highly invasive GB16 and GB42 lines have significantly higher levels of CD44 as compared to the less-invasive GB7 line. Furthermore, we sorted for CD44^{high} and CD44^{low} populations by fluorescence-activated cell-sorting from the GB42 GSC line and performed qRT-PCR for migration /invasion genes (Figure S6H). We found that the CD44^{high} population expressed high levels of migration/invasion genes, including *TGFβ2*, *ZEB1*, and *VIM*, as well as *OLIG2*, in contrast to the CD44^{low} population (Figure S6I).

Modulating TGF-β2 Levels Alters OLIG2-Mediated Glioma Invasion

To determine whether TGF-β2 is the downstream effector of OLIG2-mediated invasion in hGSCs with pOLIG2^{low}, we treated hGSCs (GB7 and GB16) with TGF-β receptor 1/2 inhibitor (TβRI) (LY2109761) for 8 hr. In parallel experiments, we supplemented the media with TGF-β2. The number of invading GB7 cells increased significantly in presence of TGF-β2, a phenotype not seen in GB16 cells (Figures 7A, 7B, S7A, and S7B). Following inhibitor treatment, there was a significant decrease in invasion in the GB16 hGSC line; however, the TβRI only had a minor effect on the less-invasive cell line (GB7) (Figures 7A, 7B, S7A, and S7B). The concentration and duration of the TβRI treatment and of TGF-β2 addition were sufficient to affect TGF-β signaling, as seen by changes in pSMAD2/3 levels and by the expression of invasion genes (Figures S7C and S7D). This effect was not due to a decrease in cell viability following TβRI treatment (Figure S7E). It is intriguing that we did not see an increase in the invasion of GB16 in the presence of external TGF-β2. It is possible that either the TGF-β2 signaling has reached its threshold or GB16 invasion is independent of SMAD2 activation. To further confirm a direct role of secreted TGF-β2, we pretreated pOLIG2^{high} hGSCs (GB7 and BT145) with conditioned media from invasive hGSC lines (GB16 and BT147) that have high levels of TGF-β2. As expected, the number of cells invading through Matrigel increased when grown in the presence of conditioned media from GB16 and BT147 (Figures 7C, 7D, S7F, and S7G). To confirm that the increased invasion was due to secreted TGF-β2 in the conditioned media, we performed migration assay with cells pretreated with both GB16 and BT147-conditioned media and TβRI. GB7 and BT145 cells failed to respond to conditioned media and displayed a significant decrease in invasion in the presence of the TβRI (Figures 7C, 7D, S7F, and S7G). These data suggest that TGF-β2 is a downstream target of OLIG2 and that inhibition of the TGF-β pathway blocks OLIG2-mediated invasion.

We tested whether OLIG2 phosphorylation/dephosphorylation is required for invasion by overexpressing TPM mutant of Olig2 in the invasive GB16 cells and TPN mutant in the less-invasive BT145 cells. Increased expression of TPM mutant in GB16 led to a dramatic decrease in the rate of invasion through Matrigel and decreased the expression of invasion markers (Figures 7E, S7H, and S7J). Conversely, overexpression of the TPN form of Olig2 in BT145 led to increased invasion, as well as the expression of invasion markers (Figures 7F, S7I, and S7K).

DISCUSSION

One of the hallmark features of glioblastoma is the infiltration of tumor cells into normal brain regions. These invasive glioma cells are the primary cause for tumor recurrence and poor prognosis in GBM patients. Understanding the molecular mechanisms and signaling pathways that trigger the invasive phenotype is critical for the development of effective treatment of GBM. Our findings provide insight into how the post-translational modification of a single TF could possibly mediate the switch between proliferative and invasive phenotypes. We show that the

Figure 4. GBM Cells Expressing Unphosphorylated OLIG2 (or pOLIG2 ^{low}) Are Infiltrative and Are Found at the Tumor Core and Rim

(A–G) Analysis of tumor cell invasion in GBM xenograft models (GB3, GB16, and BT145) 3 weeks post-implantation. Immunostaining of tumor tissue with human-specific mitochondrial antibody (green) in GB3 (A and A'), GB16 (B and B'), and BT145 (C and C'). Scale bars, 1 mm and 50 μm. Immunodetection of GB3 tumor cells away from injection site within the white matter tracts (D and D'). Scale bars, 1 mm and 100 μm. The distance traveled by tumor cells from the graft site to the anterior or posterior regions (n = 3 for each group) is shown (E). OLIG2+ cells are found throughout the tumor tissue. Quantification (F) and immunodetection (G) of OLIG2+ (red) and Ki67+ (green) cells (both single- and double-labeled cells) in GBM patient tissue section. Proliferating cells in human GBM tissue express pOLIG2.

(H and I) Quantification (H) and immunostaining (I) with pOLIG2 (red) and Ki67 (green) antibodies (both single- and double-labeled cells) in GBM patient tissue sections (DAPI, blue). Images are representative of five GBM cases (G and I). For (F) and (H), the total number of cells from five individual fields per patient tumor tissue section were counted. Scale bars, 100 μm. The analysis of glioma invasion TMA immunostained with OLIG2 and Ki67 antibodies is shown.

(J) Immune reactivity score (IRS) quantification of OLIG2+ and Ki67+ cells across 33 patient tumor core, edge, and rim in GBM patient TMA (both individual and coexpressing cells).

(K) Representative images of OLIG2 (green) and Ki6 (red) staining from core, edge, and rim in TMA sections. Scale bar, 50 μm. For all bar graphs, data represent mean ± SD from multiple experiments.*$p < 0.05$; **$p < 0.01$; ***$p < 0.001$.

See also Figure S4.

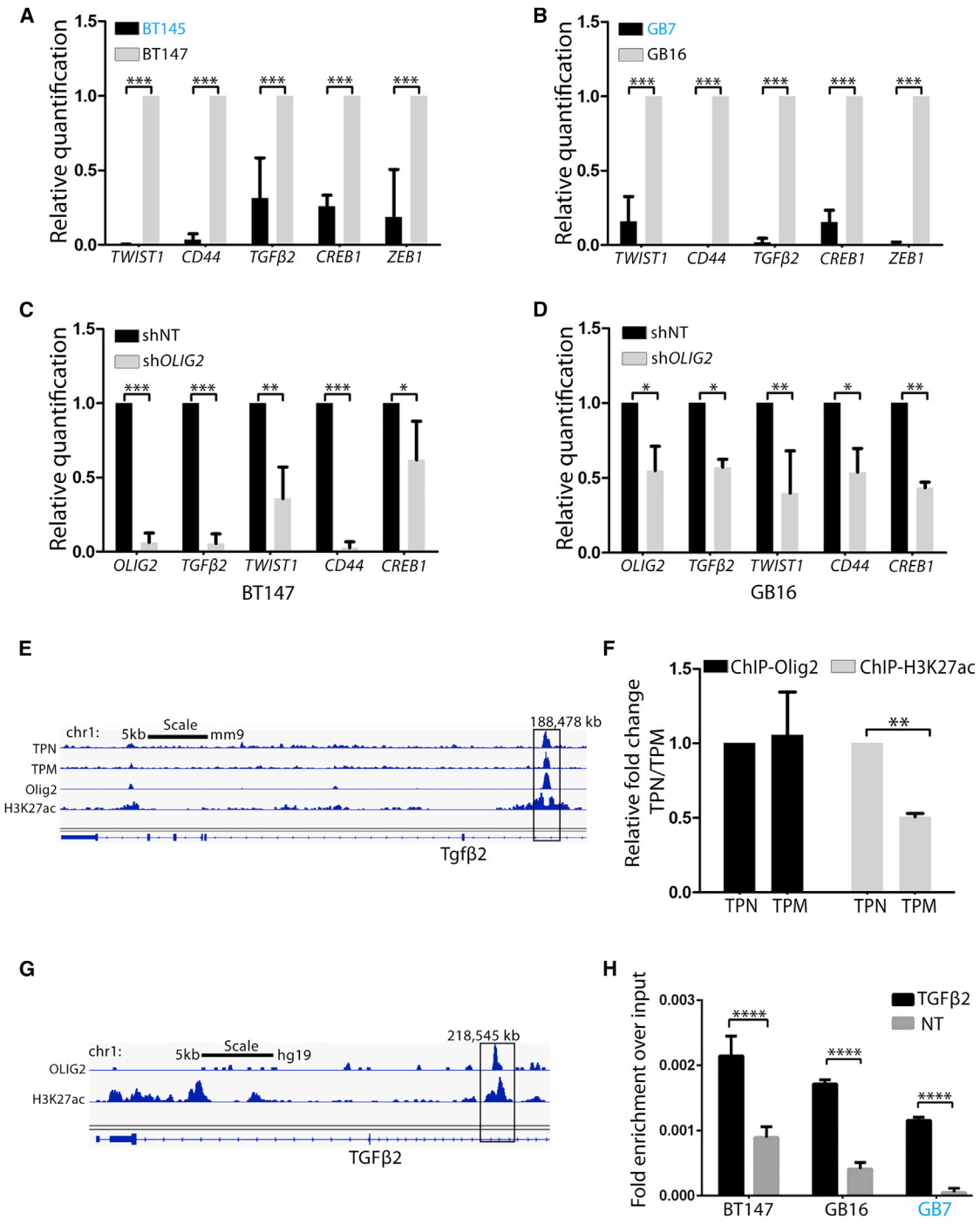

Figure 5. OLIG2 Phosphorylation-Dependent Regulation of Invasion Markers in Human GSCs

(A and B) qRT-PCR analysis of invasion genes in hGSCs with pOLIG2^{high} (BT145 and GB7) as compared to hGSCs with pOLIG2^{low} (BT147 and GB16).

(C and D) qRT-PCR in BT147 and GB16 cells transduced with either control (shNT) or sh*OLIG2*-expressing lentivirus.

(E) ChIP-seq tracks show TPN, TPM, Olig2, and H3K27ac signals at *Tgfβ2* loci (Mateo et al., 2015).

(F) Directed ChIP assay with anti-Olig2 and anti-H3K27ac to assess binding to *Tgfβ2* enhancer region in TPM- and TPN-expressing cells. Bar graph represents fold change of TPM over TPN.

(G) ChIP-seq tracks from Suvà et al. (2014) show Olig2 and H3K27ac signals at *TGFβ2* loci.

(H) Directed ChIP assay for OLIG2 binding to *TGFβ2* enhancer region in represented hGSCs as compared to the non-target site (NT). Bar graphs represent fold enrichment of OLIG2 over non-target (NT). For (A)–(D), F, and H, the data represent mean ± SEM of three independent experiments. *p < 0.05; **p < 0.01; ***p < 0.001. See also Figure S5.

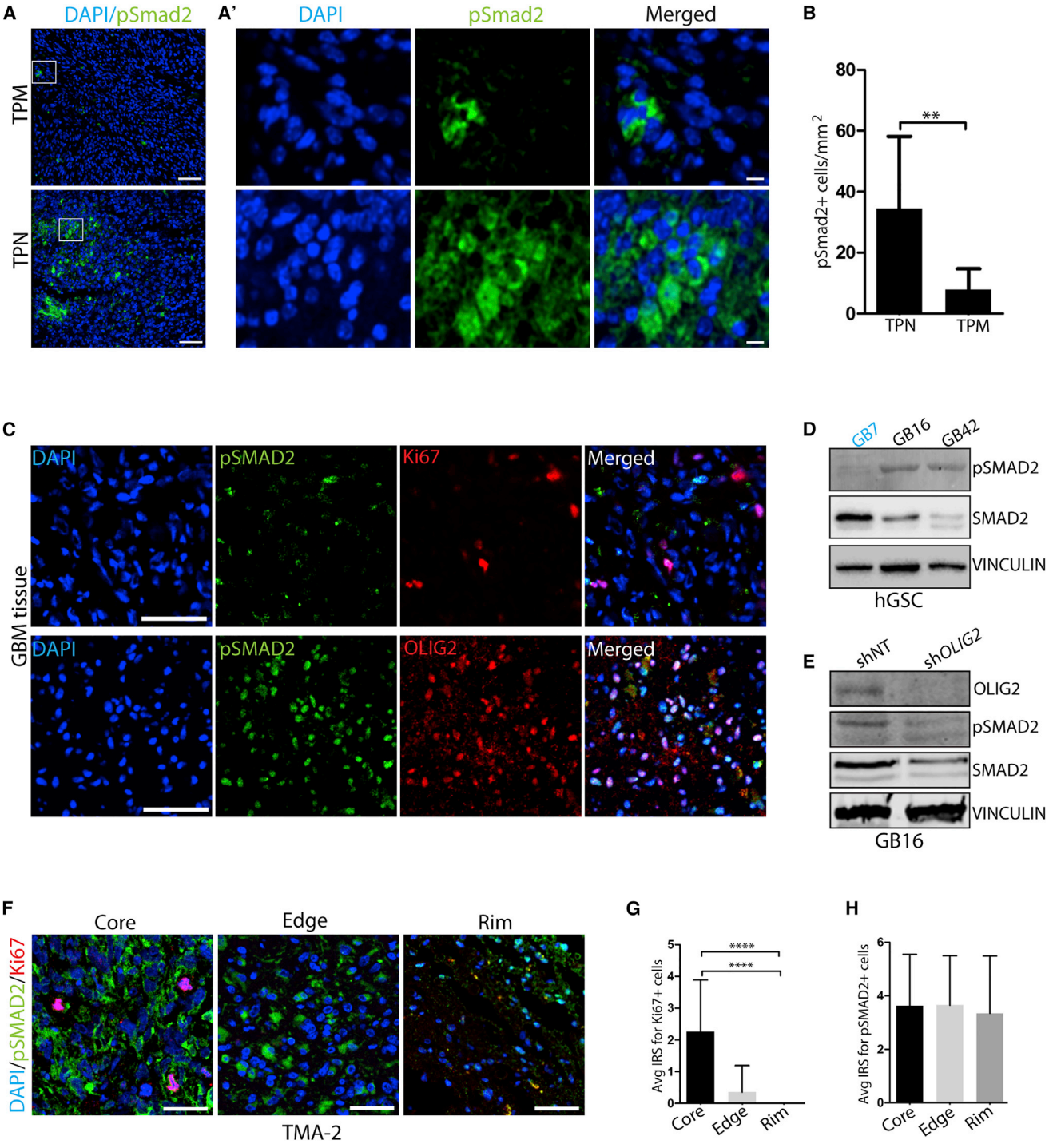

Figure 6. SMAD2 Phosphorylation Is Inversely Correlated with the High Expression of pOLIG2

(A) Immunodetection of pSmad2 (green) in orthotopic tumors induced by mGSCs expressing TPM (upper) or TPN (lower) mutant. (A') Right subpanels show higher magnification images in the boxed area from (A).

(B) Quantification of pSmad2+ cells in TPN and TPM tumor tissues (cells from five independent fields from three tumor tissues each were counted).

(C) Representative images from immunostaining of consecutive patient GBM tissue sections with pSMAD2 (green) /Ki67 (red) and pSMAD2 (green) /OLIG2 (red) antibodies. DAPI staining in blue.

(D) Western blot analysis of indicated hGSC lysates for pSMAD2 expression.

(E) Western blot analysis for OLIG2, pSMAD2, and SMAD2 after transduction with shNT or sh*OLIG2* lentivirus in GB16 cells.

(legend continued on next page)

phosphorylation status of the CNS-specific factor OLIG2 regulates glioma cell proliferation and invasion. Specifically, we have discovered that unphosphorylated OLIG2 promotes glioma invasion through the TGF-β2 signaling pathway.

Olig2 expression has been previously linked to migration/invasion, both in normal and in malignant cells (Hornig et al., 2013; Nevo et al., 2014; Siebzehnrubl et al., 2013). However, our report demonstrates that the phosphorylation status of OLIG2 regulates the switch from proliferation to invasion (Figure 7G). Recently, two studies have reported the role of OLIG2 in glioma invasion. Siebzehnrubl et al. (2013) have identified ZEB1 as a key regulator of GBM invasion and stemness. These authors have shown that ZEB1 upregulates expression of both EMT genes and critical GSC markers like SOX2 and OLIG2. Consistent with their observation, we have found that mGSCs expressing TPN and hGSCs expressing pOLIG2^{low} have high levels of invasion genes, including *ZEB1* (Figures 5 and S5). Furthermore, our findings demonstrate that ZEB1 is a direct genetic target of OLIG2, suggesting a cross-regulatory loop wherein unphosphorylated OLIG2 leads to increase in ZEB1, which, in turn, upregulates OLIG2 expression.

Another study has identified *OLIG2* as one of the genes highly expressed within the tumor cells in the invasive niche, but not at the tumor core (Nevo et al., 2014). The authors have found that in a single patient-matched tumor core versus rim, OLIG2 protein is predominantly found at the tumor rim. In contrast, previous reports (Venere et al., 2015) and our analysis of multiple human GBM fresh frozen sections and GBM invasion TMA (containing 33 matched core, edge, and rim tumor tissues) reveal that OLIG2-expressing cells are found both at the tumor core and at the peritumoral rim (~70% of tumors showed a strong signal for OLIG2 at the core, edge, and rim) (Figure 4). It is plausible that the presence of OLIG2+ cells at the tumor core and rim depends on the tumor location and the molecular subtype of the tumor. However, our analysis of more than 33 human GBM tumors, as well as observations made by other laboratories (Venere et al., 2015), suggests that OLIG2-expressing cells are present throughout the tumor. In agreement with our observations, Nevo et al. (2014) have demonstrated that the knockdown of *OLIG2* leads to a decrease in expression of the EMT gene, *TWIST1*.

The main question our data addresses is how OLIG2 can promote both proliferation and invasion. With the use of TPM and TPN mutants, we have demonstrated that phosphorylation of N-terminal serines in Olig2 decreases migration/invasion, both in normal and in malignant neural progenitors, in vitro and in vivo (Figures 1, 2, and 3). Our genetically relevant murine glioma model allows us to dissect the role of Olig2 phosphorylation in glioma invasion without the compounding effect of human genetic and epigenetic heterogeneity in GBM. We have previously shown that TPM-expressing glioma cells are highly proliferative and tumorigenic and can form tumors, even following the injection of 100 cells (Sun et al., 2011). Here, we have provided evidence for a role of unphosphorylated Olig2 in promoting tumor invasion. TPN-expressing cells form highly invasive tumors, wherein tumor cells show extensive infiltration of normal brain at distant sites (Figures 3 and S3).This is not observed in TPM-induced tumors. The only difference between these tumors is the phosphorylation status of Olig2. Xenografts of hGSCs with low levels of OLIG2 phosphorylation confirm our observations with the murine glioma model. Based on our in vivo PDX data and analysis of TMA, it seems likely that either of these two scenarios or a combination of the two exists: (1) distinct populations of GSCs within a single tumor express pOLIG2^{high}, pOLIG2^{low}, or no OLIG2 at all, and this expression is responsible for highly proliferative (pOLIG2^{high}), invasive OPC-like (OLIG2^{low}), and astrocyte-like invasive (no OLIG2) cells, or (2) within the tumor cells, OLIG2 expression and phosphorylation is modulated by the location of the tumor and/or extracellular cues from the microenvironment and other tumor cells. Analysis of a small cohort of hGSCs suggests that OLIG2 phosphorylation levels are lower in the proneural subtype of GBMs, with PDGFRa expression compared to the classical subtype with high EGFR levels (R.K. and S.M., unpublished data). However, the ectopic overexpression of Olig2 phosphomutants in hGSCs suggests that altering OLIG2 phosphorylation alone is capable of switching the phenotype from proliferative to invasive and vice versa, suggesting that both scenarios might occur in GBM tumors.

The TGF-β pathway has been shown to play an important role in invasion of tumor cells in several solid cancers, including GBM (Anido et al., 2010; Rich, 2003; Weller et al., 2001; Wick et al., 2001). Several studies have implicated the TGF-β pathway in glioma pathobiology, with high levels of both TGF-β1 and TGF-β2 being found in GBM tumors compared to normal healthy brain (Platten et al., 2001; Rich, 2003; Wick et al., 2001). Recently, high levels of *TGFβ2* expression were reported to be correlated with a poor prognosis in GBM patients (Rodón et al., 2014). Our data provide evidence that TGF-β2 acts downstream of OLIG2 and is a critical player in promoting OLIG2-mediated glioma invasion. hGSCs with pOLIG2^{low} express high levels of pSMAD2 protein, which is one of the mediators of TGF-β signaling (Figure 6). High levels of pSMAD2 expression in GSCs with low or unphosphorylated OLIG2 suggest that GBM tumor cells that have pOLIG2^{low} levels are inherently more invasive because of an active TGF-β2 pathway.

Previous studies have demonstrated the importance of TGF-β signaling in the maintenance of the mesenchymal stem-like population in GBM cells (Anido et al., 2010). Our study provides the mechanism involved in the regulation of TGF-β levels in hGSCs through the modulation of OLIG2 phosphorylation (Figure 7). Overexpression of Olig2 phosphomutants (pOLIG2^{high}) suggests that the presence of pOLIG2 suppresses the invasion program, in part through the suppression of *TGFβ2* signaling pathway.

(F–H) Representative images of Ki67 and pSMAD2 immunostaining at core, edge, and rim regions in TMA-2 (F). IRS quantification of Ki67+ (red) (G) and pSMAD2+ (green) (H) cells at core, edge, and rim regions (see the Experimental Procedures for details). DAPI is in blue. Scale bars, 50 (A), 5 (A') 100, (C) and 50 μm (F). For bar graphs in (B), (G), and (H), data represent mean ± SEM. *p < 0.05; **p < 0.01; ***p < 0.001.
See also Figure S6.

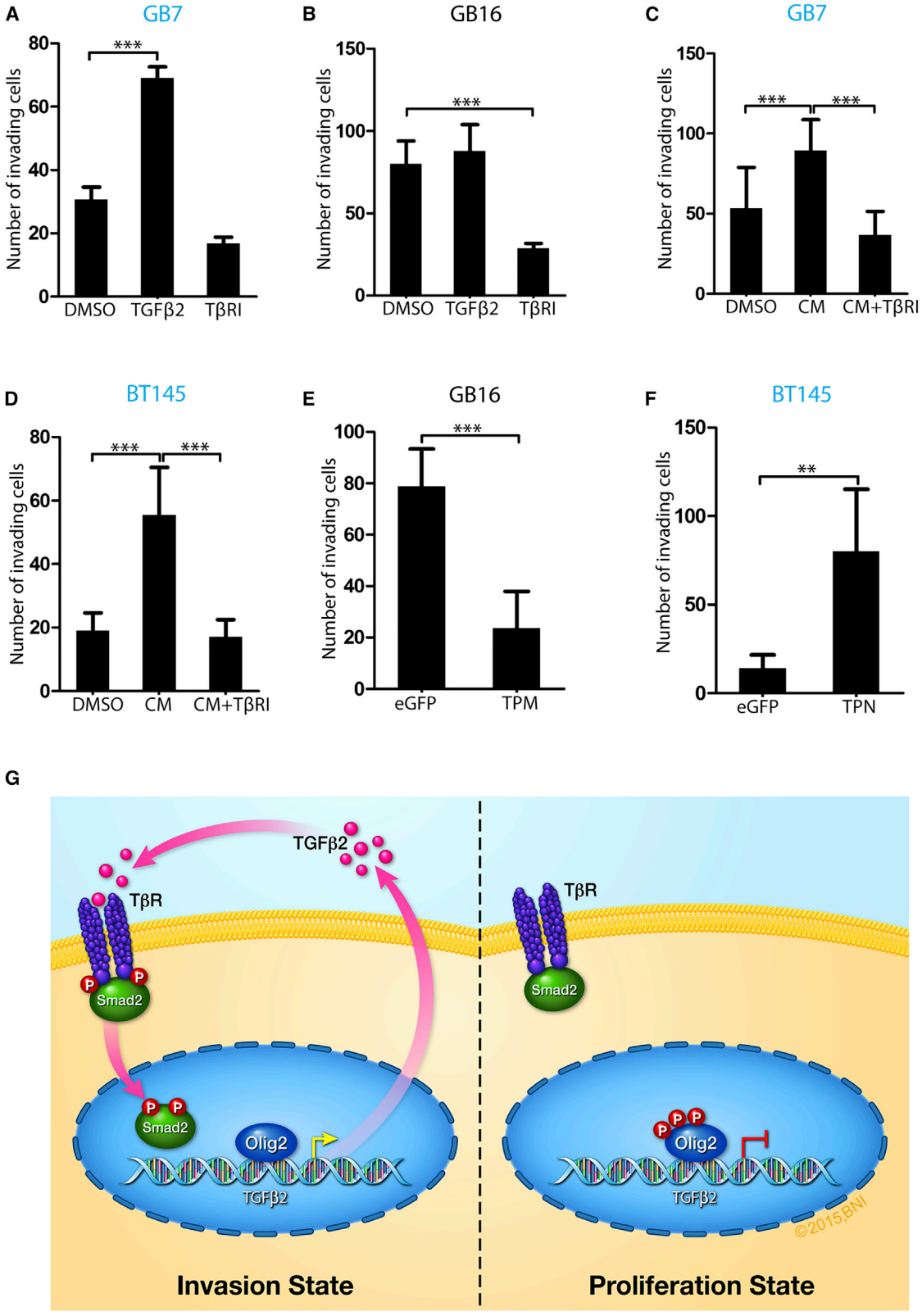

(legend on next page)

OPCs are the major proliferating cell population in adult brain (Dawson et al., 2003; Geha et al., 2010). Following brain injury, OPCs migrate to the site of injury and contribute to scar formation and remyelination (Hughes et al., 2013). Given the fact that Olig2 plays an important role in OPC specification, it is not surprising that overexpression of Olig2 in OPCs enhances migration (Hornig et al., 2013). Our data suggest that glioma cells exploit Olig2's normal role in OPC migration to invade and populate normal brain parenchyma.

Collectively, our experimental findings provide insight into how a single TF can lead to either tumor growth or invasion, depending on its phosphorylation state. The role of OLIG2 (a critical factor for gliomagenic properties of GSCs) in GBM invasion provides strong support to the presence of glioma stem-like cells at the invasive rim. The OLIG2+ therapy-resistant cells that evade surgical resection could be the likely source of tumor recurrence in GBM. Although therapies targeting glioma invasion alone have shown no clinical benefit, our data provide strong support for adjuvant therapies, in conjunction with anti-proliferative agents, that can target invasive cells. Several agents targeting the TGF-β pathway, including an antisense oligonucleotide against TGF-β2 (AP-12009), are currently being evaluated in clinical trials for high-grade gliomas (Joseph et al., 2013). Future combination studies with inhibitors of OLIG2 phosphorylation and the TGF-β2 pathway will shed light on the therapeutic effectivenessof targeting both pOLIG2 and unphosphorylated OLIG2.

EXPERIMENTAL PROCEDURES

Cell Culture

The patient samples used for this research were provided by the Biobank Core Facility at St. Joseph's Hospital and Medical Center and Barrow Neurological Institute (BNI). The samples were deidentified and conformed to the Biobank Institutional Review Board's protocol. Patient-derived cell lines (GB3, GB7, GB16, and GB42) were established from resected primary GBM tumor tissue at BNI. BT145 and BT147 cells were obtained from K.L.L.'s laboratory at the Dana-Farber Cancer Institute and propagated under similar conditions. Both mGSCs and hGSCs were cultured, as described previously (Ligon et al., 2007; Mehta et al., 2011). Tumor-bearing animals were euthanized at the onset of neurological symptoms. See the Supplemental Experimental Procedures for details.

Animal Experiments

Animal husbandry was performed in accordance with the guidelines of the St. Joseph Hospital and Medical Center and Barrow Neurological Institute under the protocol approved by the Institutional Animal Care and Use Committee. 5- to 6-week-old CrTac: NCr-*Foxn1*^{nu} nude mice (Taconic Biosciences) were used for in vivo orthotropic transplant of BT145, GB3, and GB16 cells. Mouse tumor tissues derived from the injection of TPM and TPN-expressing cells were obtained from Dr. Sun (C.D. Stiles laboratory) at the Dana-Farber Cancer Institute. BT145 and BT147 xenograft tissues were obtained from K.L.L.'s laboratory at the Dana-Farber Cancer Institute. For orthotopic transplants, 2 μl of dissociated cells at a density of 100,000 cells/μl were injected in the right striatum, as described previously (Ligon et al., 2007; Mehta et al., 2011).

Tissue Processing and Cell Culture

Tissue was disaggregated using the gentleMACS Dissociator and enzymatically digested with a Tumor Tissue Dissociation Kit with papain (Miltenyi Biotec). Cells were plated at a density of 5 × 10^5 to 1 × 10^6 cells in Corning non-tissue culture-treated 75-cm^2 flasks. mNSCs, mGSCs, and hGSCs were cultured as spheres on non-tissue culture-treated flasks or as adherent cultures on laminin (Sigma-Aldrich) in DMEM/F12 media, supplemented with B27 and N2 (Invitrogen; ThermoFisher Scientific) in the presence of 20 ng/ml epidermal growth factor (EGF) and basic fibroblast growth factor (bFGF) (EMD Millipore; Merck).

Immunofluorescence

For mouse brain tissue, immunofluorescence was performed on free-floating sections (40 μm thickness), while for human, frozen tumor tissue sections (5 μm thickness) were utilized. For TPN/TPM and BT145/BT147 FFPE tumor tissues, 5-μm thickness sections were used. For immunodetection of nuclear antigens, tissues were treated for 45 min in citrate buffer (pH 6) at 80°C. For detailed staining procedures, see the Supplemental Experimental Procedures.

Imaging

Analysis of immunostaining was performed on confocal stacks (with a step size of 1 μm) acquired with a 20× oil-immersion objective on a laser-scanning microscope (Leica; Leica Microsystems).

Analysis of Migratory Properties of GBM Lines

We injected 100,000 cells of two pOLIG2^{low} lines (GB16 and GB3) and one −pOlig2^{high} line (BT145) as described above. After 24 days, the mice (n = 3 per group) were sacrificed, and brains were fixed as described above. Following 30% sucrose treatment, brains were frozen and cut into 40-μm sections using a cryostat. Sections were collected in 1:8 series so that in each series, consecutive sections were spatially separated by 280 μm. After staining with anti-hMitochondria and anti-VIMENTIN, sections were mounted on gelatin-coated slides (LabScientific) in a thorough antero-posterior anatomical order. Cancer cells were identified by the co-expression of hMitochondria and VIMENTIN. The maximum distance reached by GBM cells was calculated as 280 μm multiplied by the number of sections separating the section with a visible needle track and the furthermost anterior and posterior sections containing hMito+/VIM+ cells.

Real-Time PCR and ChIP Analysis

Total RNA was extracted from cells by using the RNeasy Purification Kit (QIAGEN) in accordance with the manufacturer's instructions. RNA was quantified on a NanoDrop Spectrophotometer (Thermo Scientific; ThermoFisher

Figure 7. OLIG2 Promotes Glioma Invasion via the TGF-β2 Pathway

(A) Number of invading cells showing increased invasion following TGF-β2 addition or reduced invasion following TβRI treatment in less-invasive GB7 cells.
(B) Quantification showing reduced invasion following TβRI treatment in GB16 cells.
(C and D) Increase in invading GB7 cells in the presence of conditioned media from invasive GB16 (C). Increase in invading BT145 cells in the presence of conditioned media from invasive BT147 cells (D). The addition of TβRI to conditioned media reduces invasion.
(E) GB16 cells show impaired invasion when transduced with TPM-expressing lentivirus compared to control eGFP virus.
(F) BT145 cells showed a significant increase in invasion when transduced with TPN-expressing lentivirus compared to eGFP control virus.
(G) Model of Olig2 phosphorylation-dependent glioma invasion. Our results suggest that when OLIG2 is phosphorylated at the N terminus, the TGF-β2 levels are low, and hence there is no phosphorylation of SMAD2. Unphosphorylated OLIG2 triggers expression of TGF-β2, which then associates with TGF-βR1/2, resulting in phosphorylation and nuclear localization of SMAD2 and eventual increase in invasion. For all graphs, data represent mean ± SD of three independent experiments. *$p < 0.05$; **$p < 0.01$; ***$p < 0.001$).
See also Figure S7.

Scientific), and 1 μg of total RNA was used for cDNA synthesis by using the SuperScript III Kit (Life Technologies). qPCR was performed using inventoried TaqMan assays for respective target genes and housekeeping control genes (HPRT or 18S) on the QuantStudio 6 Flex Real-Time PCR System (Life Technologies; ThermoFisher Scientific). ChIP experiments were performed as described previously (Meijer et al., 2014). Primer details are provided in the Supplemental Experimental Procedures.

GBM Subtype Classification of Human GSCs

Human GSC lines from K.L.L.'s laboratory (BT145 and BT147) have been classified by genetic mutations, microarray analysis, and array CGH analysis. GB lines have been classified by qRT-PCR analysis of genes associated with each subtype (Verhaak et al., 2010) using inventoried Taqman assays (*PDGFRa*, *DLL3*, *OLIG2*, *PTEN*, *TOP2A*, *EGFR*, *CD44*, and *CHI3L1*). It is important to note that Table S1 indicates the proteins levels of OLIG2. IDH1 mutation status was confirmed by the pathology department at St. Joseph's Hospital and Medical Center by immunohistochemistry with anti-IDH1R132H antibody. Samples were classified into a particular subtype by the expression of most markers within a subtype.

Cell Migration and Invasion Assay

For determination of migration capacity, 10,000 cells/well (mNSC, mGSC and hGSC) were seeded on the laminin-coated 96-well Oris Cell Seeding Stoppers or on an Oris (BCG) plate (Platypus Technologies). The stoppers were removed after 2 hr, and additional media with growth factors were added to the wells. The migration of cells to the detection zone was analyzed after 24 hr. Cells were imaged using bright-field microscopy. Images were then analyzed for cell migration using ImageJ software (NIH, U.S. Department of Health and Human Services). The invasion potential was determined on collagen-coated transwell inserts with a pore size of 8 μm (Becton Dickinson). Dissociated cells (~100,000/well for mNSC or mGSC) and (~50,000/well for hGSC) were resuspended in serum-free media with growth factors (20 ng/ml EGF and bFGF each) and mixed with thawed Matrigel (BD Biosciences). A total of 50 μl of Matrigel plus cells suspension was transferred to transwells and inserted in triplicates; transwells were then placed in 24-well plates. After 24 (for hGSC) or 48 hr (for mNSC or mGSC), invaded cells that accumulated on the bottom surface of the transwell insert membrane were fixed with 4% PFA (paraformaldehyde) for 20 min and stained with DAPI for 1 min. The membranes were subsequently cut out and mounted on microscopic slides for quantification. Representative pictures of the membranes with cells were acquired at 10× or 20× magnifications, and the total number of cells in five individual fields per membrane was counted; the mean ± SD number of invading cells for every condition was calculated. Cells were treated with TGF-β2 (10 ng/ml; GIBCO; ThermoFisher Scientific) and/or the small-molecule inhibitor of TβRI/II, LY2109761 (2 μM; ApexBio Technology; Fisher Scientific; ThermoFisher Scientific).

Quantification of TGF-β2 by ELISA

Levels of TGF-β2 secreted by murine or human cells in cell-culture media were measured using sandwich ELISA (Quantikine mouse TGF-β2 and Quantikine human TGF-β-2; R&D Systems) in accordance with the manufacturer's protocol. Cells were seeded (1×10^5 cells/well, 24-well plates) on laminin-coated plates and incubated for 36 hr. The values were expressed as nanograms per milligram of protein.

TMA Staining and Analysis

Glioma invasion tissue microarrays (TMAs) were obtained from M.E.B. laboratory at TGen (Kislin et al., 2009). Slides were deparaffinized and hydrated, followed by heat-mediated antigen retrieval in 10 mM citrate buffer (pH 6) at 80°C, and subsequently immunostained with fluorescence-conjugated antibodies as described above. For each immunostaining, TMA were imaged with a 20× oil-immersion objective. In this study 33 patient tumor tissues on the TMA were used for the analysis of the percentage of positive cells at the core, rim, or edge. The closest H&E section from the TMA was reviewed by Dr. Jennifer Eschbacher, a board-certified neuropathologist at the St. Joseph's Hospital & Medical Center. The TMA images were assessed and scored in accordance with the semiquantitative scoring system to obtain the immunoreactive score (IRS) (Remmele and Stegner, 1987). For evaluation of the staining patterns, the percentage of positive cells (PP; zero points: no positive cells, one point: 1%–10%, two points: 10%–20%, three points; >20%) and the staining intensity (SI; 0 point: no signal, 1 point: weak, 2 point: moderate, 3 point; strong) was determined and added. The average IRS score was plotted for each staining.

Statistical Analyses

Data are presented as the mean ± SD or as the mean ± SEM. If comparing two conditions or cell lines, significance was tested with unpaired two-tailed Student's t test. Significance of the differences between conditions or cell lines was tested by the two-way ANOVA with Bonferroni multiple comparison tests using GraphPad Prism software. Statistical significance was defined as $p < 0.05$.

For detailed methods, see the Supplemental Experimental Procedures.

SUPPLEMENTAL INFORMATION

Supplemental Information includes Supplemental Experimental Procedures, seven figures, and one table and can be found with this article online at http://dx.doi.org/10.1016/j.celrep.2016.06.045.

AUTHOR CONTRIBUTIONS

S.M. and S.K.S. conceived and designed the experiments and wrote the manuscript. S.K.S. standardized the techniques and performed most of the experiments and analyzed data. S.K.S and R.F. performed the immunohistochemistry experiments with xenograft tissues, analyzed the data, and edited the manuscript; R.K. produced the lentivirus, generated stable cell lines, and helped characterize patient-derived GBM lines; S.K.S and S.R. isolated RNA, performed the qPCR analysis, and analyzed the immunofluorescence images; E.S. cultured PDX GBM lines, assisted in intracranial surgeries, and performed the ELISA; S.K.S. and C.L. generated the lentivirus, performed the invasion assays, and performed the intracranial surgeries; C.L.M. provided the patient-derived cells, the xenograft tissue, and edited the manuscript; Y.S. provided murine xenograft tissues; J.A.A. provided the antibodies, various constructs, and reagents and edited the manuscript; J.M.E. provided the patient tissue for analysis, conducted neuropathological analysis of H&E samples for GBM tissue, and helped with scoring of TMA; K.L.L. provided the patient-derived cells and PDX tissues from DFCI; M.E.B. provided the glioma invasion TMA; N.S. provided the patient-derived tissues; and S.M. coordinated the project, helped analyze the data, and wrote the manuscript.

ACKNOWLEDGMENTS

Patient-derived glioma cells were provided by the Biobank Core Facility at St. Joseph's Hospital and Barrow Neurological Institute and the Living Tissue Bank at Dana-Farber Cancer Institute. The biobank is funded by the Arizona Biomedical Research Commission and the Barrow Neurological Foundation. We are grateful to Dr. Mythreye Karthikeyan (University of South Carolina at Columbia) for useful suggestions for the ELISA and the TGF–β signaling, in general. We thank Timothy Troxel, Dr. Sara Bowen, Jonathan Yamaguchi, Lior Shtayer, Nicole Giannonatti, Laura Belmont, and Padhmavathy Yuvaraj for their technical assistance. Dr. Harshil Dhruv and Brock Armstrong (TGen) provided the reagents and technical advice for the glioma tissue microarray. We thank the Neuro publications department at the Barrow Neurological Institute for their help with the illustrations. This work was supported by the Barrow Neurological Foundation (to S.M.). S.M is also supported by an NIH/NINDS grant (R01 NS088648A) and the Bear Necessities Pediatric Cancer Foundation. N.S. is supported by NIH grants (R01 NS082745 and R01 CA175391).

Received: January 8, 2016
Revised: April 28, 2016
Accepted: June 9, 2016
Published: July 7, 2016

REFERENCES

Anido, J., Sáez-Borderías, A., Gonzàlez-Juncà, A., Rodón, L., Folch, G., Carmona, M.A., Prieto-Sánchez, R.M., Barba, I., Martínez-Sáez, E., Prudkin, L., et al. (2010). TGF-β receptor inhibitors target the CD44(high)/Id1(high) glioma-initiating cell population in human glioblastoma. Cancer Cell *18*, 655–668.

Carro, M.S., Lim, W.K., Alvarez, M.J., Bollo, R.J., Zhao, X., Snyder, E.Y., Sulman, E.P., Anne, S.L., Doetsch, F., Colman, H., et al. (2010). The transcriptional network for mesenchymal transformation of brain tumours. Nature *463*, 318–325.

Cayre, M., Canoll, P., and Goldman, J.E. (2009). Cell migration in the normal and pathological postnatal mammalian brain. Prog. Neurobiol. *88*, 41–63.

Dawson, M.R., Polito, A., Levine, J.M., and Reynolds, R. (2003). NG2-expressing glial progenitor cells: an abundant and widespread population of cycling cells in the adult rat CNS. Mol. Cell. Neurosci. *24*, 476–488.

Dhruv, H.D., McDonough Winslow, W.S., Armstrong, B., Tuncali, S., Eschbacher, J., Kislin, K., Loftus, J.C., Tran, N.L., and Berens, M.E. (2013). Reciprocal activation of transcription factors underlies the dichotomy between proliferation and invasion of glioma cells. PLoS ONE *8*, e72134.

Furnari, F.B., Fenton, T., Bachoo, R.M., Mukasa, A., Stommel, J.M., Stegh, A., Hahn, W.C., Ligon, K.L., Louis, D.N., Brennan, C., et al. (2007). Malignant astrocytic glioma: genetics, biology, and paths to treatment. Genes Dev. *21*, 2683–2710.

Geha, S., Pallud, J., Junier, M.P., Devaux, B., Leonard, N., Chassoux, F., Chneiweiss, H., Daumas-Duport, C., and Varlet, P. (2010). NG2+/Olig2+ cells are the major cycle-related cell population of the adult human normal brain. Brain Pathol. *20*, 399–411.

Giese, A. (2003). Glioma invasion–pattern of dissemination by mechanisms of invasion and surgical intervention, pattern of gene expression and its regulatory control by tumorsuppressor p53 and proto-oncogene ETS-1. Acta Neurochir. Suppl. (Wien) *88*, 153–162.

Giese, A., Loo, M.A., Tran, N., Haskett, D., Coons, S.W., and Berens, M.E. (1996). Dichotomy of astrocytoma migration and proliferation. Int. J. Cancer *67*, 275–282.

Giese, A., Bjerkvig, R., Berens, M.E., and Westphal, M. (2003). Cost of migration: invasion of malignant gliomas and implications for treatment. J. Clin. Oncol. *21*, 1624–1636.

Glas, M., Rath, B.H., Simon, M., Reinartz, R., Schramme, A., Trageser, D., Eisenreich, R., Leinhaas, A., Keller, M., Schildhaus, H.U., et al. (2010). Residual tumor cells are unique cellular targets in glioblastoma. Ann. Neurol. *68*, 264–269.

Gupta, P.B., Onder, T.T., Jiang, G., Tao, K., Kuperwasser, C., Weinberg, R.A., and Lander, E.S. (2009). Identification of selective inhibitors of cancer stem cells by high-throughput screening. Cell *138*, 645–659.

Hess, K.R., Wong, E.T., Jaeckle, K.A., Kyritsis, A.P., Levin, V.A., Prados, M.D., and Yung, W.K. (1999). Response and progression in recurrent malignant glioma. Neuro-oncol. *1*, 282–288.

Hornig, J., Fröb, F., Vogl, M.R., Hermans-Borgmeyer, I., Tamm, E.R., and Wegner, M. (2013). The transcription factors Sox10 and Myrf define an essential regulatory network module in differentiating oligodendrocytes. PLoS Genet. *9*, e1003907.

Hughes, E.G., Kang, S.H., Fukaya, M., and Bergles, D.E. (2013). Oligodendrocyte progenitors balance growth with self-repulsion to achieve homeostasis in the adult brain. Nat. Neurosci. *16*, 668–676.

Joseph, J.V., Balasubramaniyan, V., Walenkamp, A., and Kruyt, F.A. (2013). TGF-β as a therapeutic target in high grade gliomas - promises and challenges. Biochem. Pharmacol. *85*, 478–485.

Kalluri, R., and Weinberg, R.A. (2009). The basics of epithelial-mesenchymal transition. J. Clin. Invest. *119*, 1420–1428.

Kislin, K.L., McDonough, W.S., Eschbacher, J.M., Armstrong, B.A., and Berens, M.E. (2009). NHERF-1: modulator of glioblastoma cell migration and invasion. Neoplasia *11*, 377–387.

Ligon, K.L., Alberta, J.A., Kho, A.T., Weiss, J., Kwaan, M.R., Nutt, C.L., Louis, D.N., Stiles, C.D., and Rowitch, D.H. (2004). The oligodendroglial lineage marker OLIG2 is universally expressed in diffuse gliomas. J. Neuropathol. Exp. Neurol. *63*, 499–509.

Ligon, K.L., Huillard, E., Mehta, S., Kesari, S., Liu, H., Alberta, J.A., Bachoo, R.M., Kane, M., Louis, D.N., Depinho, R.A., et al. (2007). Olig2-regulated lineage-restricted pathway controls replication competence in neural stem cells and malignant glioma. Neuron *53*, 503–517.

Loftus, J.C., Ross, J.T., Paquette, K.M., Paulino, V.M., Nasser, S., Yang, Z., Kloss, J., Kim, S., Berens, M.E., and Tran, N.L. (2012). miRNA expression profiling in migrating glioblastoma cells: regulation of cell migration and invasion by miR-23b via targeting of Pyk2. PLoS ONE *7*, e39818.

Lu, Q.R., Park, J.K., Noll, E., Chan, J.A., Alberta, J., Yuk, D., Alzamora, M.G., Louis, D.N., Stiles, C.D., Rowitch, D.H., and Black, P.M. (2001). Oligodendrocyte lineage genes (OLIG) as molecular markers for human glial brain tumors. Proc. Natl. Acad. Sci. USA *98*, 10851–10856.

Maher, E.A., Furnari, F.B., Bachoo, R.M., Rowitch, D.H., Louis, D.N., Cavenee, W.K., and DePinho, R.A. (2001). Malignant glioma: genetics and biology of a grave matter. Genes Dev. *15*, 1311–1333.

Mani, S.A., Guo, W., Liao, M.J., Eaton, E.N., Ayyanan, A., Zhou, A.Y., Brooks, M., Reinhard, F., Zhang, C.C., Shipitsin, M., et al. (2008). The epithelial-mesenchymal transition generates cells with properties of stem cells. Cell *133*, 704–715.

Mateo, J.L., van den Berg, D.L., Haeussler, M., Drechsel, D., Gaber, Z.B., Castro, D.S., Robson, P., Crawford, G.E., Flicek, P., Ettwiller, L., et al. (2015). Characterization of the neural stem cell gene regulatory network identifies OLIG2 as a multifunctional regulator of self-renewal. Genome Res. *25*, 41–56.

Mehta, S., Huillard, E., Kesari, S., Maire, C.L., Golebiowski, D., Harrington, E.P., Alberta, J.A., Kane, M.F., Theisen, M., Ligon, K.L., et al. (2011). The central nervous system-restricted transcription factor Olig2 opposes p53 responses to genotoxic damage in neural progenitors and malignant glioma. Cancer Cell *19*, 359–371.

Meijer, D.H., Kane, M.F., Mehta, S., Liu, H., Harrington, E., Taylor, C.M., Stiles, C.D., and Rowitch, D.H. (2012). Separated at birth? The functional and molecular divergence of OLIG1 and OLIG2. Nat. Rev. Neurosci. *13*, 819–831.

Meijer, D.H., Sun, Y., Liu, T., Kane, M.F., Alberta, J.A., Adelmant, G., Kupp, R., Marto, J.A., Rowitch, D.H., Nakatani, Y., et al. (2014). An amino terminal phosphorylation motif regulates intranuclear compartmentalization of Olig2 in neural progenitor cells. J. Neurosci. *34*, 8507–8518.

Nevo, I., Woolard, K., Cam, M., Li, A., Webster, J.D., Kotliarov, Y., Kim, H.S., Ahn, S., Walling, J., Kotliarova, S., et al. (2014). Identification of molecular pathways facilitating glioma cell invasion in situ. PLoS ONE *9*, e111783.

Ostrom, Q.T., Gittleman, H., Fulop, J., Liu, M., Blanda, R., Kromer, C., Wolinsky, Y., Kruchko, C., and Barnholtz-Sloan, J.S. (2015). CBTRUS statistical report: primary brain and central nervous system tumors diagnosed in the United States in 2008-2012. Neuro-oncol. *17* (*Suppl 4*), iv1–iv62.

Platten, M., Wick, W., and Weller, M. (2001). Malignant glioma biology: role for TGF-beta in growth, motility, angiogenesis, and immune escape. Microsc. Res. Tech. *52*, 401–410.

Polyak, K., and Weinberg, R.A. (2009). Transitions between epithelial and mesenchymal states: acquisition of malignant and stem cell traits. Nat. Rev. Cancer *9*, 265–273.

Remmele, W., and Stegner, H.E. (1987). [Recommendation for uniform definition of an immunoreactive score (IRS) for immunohistochemical estrogen receptor detection (ER-ICA) in breast cancer tissue]. Pathologe *8*, 138–140.

Rich, J.N. (2003). The role of transforming growth factor-beta in primary brain tumors. Front. Biosci. *8*, e245–e260.

Rodón, L., Gonzàlez-Juncà, A., Inda, Mdel.M., Sala-Hojman, A., Martínez-Sáez, E., and Seoane, J. (2014). Active CREB1 promotes a malignant TGFβ2 autocrine loop in glioblastoma. Cancer Discov. *4*, 1230–1241.

Schmierer, B., and Hill, C.S. (2007). TGFbeta-SMAD signal transduction: molecular specificity and functional flexibility. Nat. Rev. Mol. Cell Biol. *8*, 970–982.

Siebzehnrubl, F.A., Silver, D.J., Tugertimur, B., Deleyrolle, L.P., Siebzehnrubl, D., Sarkisian, M.R., Devers, K.G., Yachnis, A.T., Kupper, M.D., Neal, D., et al. (2013). The ZEB1 pathway links glioblastoma initiation, invasion and chemoresistance. EMBO Mol. Med. *5*, 1196–1212.

Silver, D.J., Siebzehnrubl, F.A., Schildts, M.J., Yachnis, A.T., Smith, G.M., Smith, A.A., Scheffler, B., Reynolds, B.A., Silver, J., and Steindler, D.A. (2013). Chondroitin sulfate proteoglycans potently inhibit invasion and serve as a central organizer of the brain tumor microenvironment. J. Neurosci. *33*, 15603–15617.

Sun, Y., Meijer, D.H., Alberta, J.A., Mehta, S., Kane, M.F., Tien, A.C., Fu, H., Petryniak, M.A., Potter, G.B., Liu, Z., et al. (2011). Phosphorylation state of Olig2 regulates proliferation of neural progenitors. Neuron *69*, 906–917.

Suvà, M.L., Rheinbay, E., Gillespie, S.M., Patel, A.P., Wakimoto, H., Rabkin, S.D., Riggi, N., Chi, A.S., Cahill, D.P., Nahed, B.V., et al. (2014). Reconstructing and reprogramming the tumor-propagating potential of glioblastoma stem-like cells. Cell *157*, 580–594.

Venere, M., Horbinski, C., Crish, J.F., Jin, X., Vasanji, A., Major, J., Burrows, A.C., Chang, C., Prokop, J., Wu, Q., et al. (2015). The mitotic kinesin KIF11 is a driver of invasion, proliferation, and self-renewal in glioblastoma. Sci. Transl. Med. *7*, 304ra143.

Verhaak, R.G., Hoadley, K.A., Purdom, E., Wang, V., Qi, Y., Wilkerson, M.D., Miller, C.R., Ding, L., Golub, T., Mesirov, J.P., et al.; Cancer Genome Atlas Research Network (2010). Integrated genomic analysis identifies clinically relevant subtypes of glioblastoma characterized by abnormalities in PDGFRA, IDH1, EGFR, and NF1. Cancer Cell *17*, 98–110.

Weller, M., Wick, W., and Platten, M. (2001). Role of TGF-beta in oncogenesis. Microsc. Res. Tech. *52*, 353.

Weller, M., Cloughesy, T., Perry, J.R., and Wick, W. (2013). Standards of care for treatment of recurrent glioblastoma–are we there yet? Neuro-oncol. *15*, 4–27.

Wick, W., Platten, M., and Weller, M. (2001). Glioma cell invasion: regulation of metalloproteinase activity by TGF-beta. J. Neurooncol. *53*, 177–185.

Wong, E.T., Hess, K.R., Gleason, M.J., Jaeckle, K.A., Kyritsis, A.P., Prados, M.D., Levin, V.A., and Yung, W.K. (1999). Outcomes and prognostic factors in recurrent glioma patients enrolled onto phase II clinical trials. J. Clin. Oncol. *17*, 2572–2578.